American Mineralogist, Volume 84, pages 144–151, 1999

Dissolution of the periclase (001) surface: A scanning force microscope study

GUNTRAM JORDAN,* STEVEN R. HIGGINS, AND CARRICK M. EGGLESTON

Department of Geology and Geophysics, University of Wyoming, Laramie, Wyoming 82071-3006, U.S.A.

ABSTRACT

In contrast to most ionic minerals studied by SFM, the periclase (001) surface dissolves not by retreat of monolayer steps parallel to (001), but by retreat of a rough surface perpendicular to (001). At pH < 2, dissolution has an additional contribution from retreating macro-steps at the edges of nearly square pits. The macro-steps have heights up to 120 nm. In general, step direction is parallel to [110] and equivalent directions. During dissolution at low pH, a soft near-surface region is formed. Other investigators have shown that the near-surface region is protonated. Protonation is supposed to stabilize the (111) surface of periclase. Due to the structural similarities between periclase (111) and brucite (001), and similar dissolution rates of periclase and brucite at pH < 5, we conclude that during dissolution the periclase (001) surface is restructured into ''(111) nano-facets'' representing brucite (001)-like layers and appearing as a rough and soft surface in SFM images. The most probable reasons that the slopes of these macro-steps (up to 50°) are lower than the slopes of perfect (111) facets are the likely poorly ordered structure of these layers, microtopography on these surface facets, and tip-surface convolution in SFM. By measuring the vertical position of the surface vs. time, we calculated the dissolution rate. At pH 1 and pH 2 we found the rates to be $17.1 \pm 5.8 \times 10^{-6}$ and $5.7 \pm 3.7 \times 10^{-6}$ mol/m^2·s, respectively. These rates are in reasonable agreement with previously reported rates of periclase and brucite (001) dissolution, and are consistent with the idea that the MgO (001) surface consists of $Mg(OH)_2$ (001)-like layers.

INTRODUCTION

Dissolution of metal-oxides and aluminosilicates is among the most crucial reactions influencing the Earth's surface by transforming rocks and soils into aqueous solutes (e.g., Sverdrup 1990; White and Brantley 1995). Such reactions can influence not only local water quality (e.g., Stumm 1985, 1987), but also global climate (Berner 1995). Recently, scanning force microscopy (SFM) has enhanced our ability to study dissolution mechanisms at a molecular level (e.g., Bosbach and Rammensee 1994; Gratz et al. 1990; Hillner et al. 1992a; Liang et al. 1996). Besides in-situ, real-time investigation of kinematics and microtopography of the solid-liquid interface with monolayer resolution, SFM also enables the acquisition of quantitative data such as the dissolution rate and the activation energy for dissolution (Jordan and Rammensee 1996, 1998). However, the dissolution rates of most oxides and silicates are too low for near-room temperature study by SFM.

One of the few oxides that allows SFM-investigation of dissolution rate and mechanism at room temperature is periclase (MgO). Due to its simple structure, MgO serves as a model oxide for studying the tendency of many oxides to transform into the more stable hydroxides under natural aqueous conditions. For MgO, this relationship is well known (e.g., Roy et al. 1953). Additionally, MgO is used as a substrate for high-temperature superconductor thin films; in this application, water can cause serious damage to both the film and the substrate (e.g., Watson et al. 1995).

This study aims to investigate the rate and mechanism of MgO dissolution, particularly the effect on dissolution of the tendency toward transformation to the hydroxide. The implications of this hydroxylation process for dissolution are poorly understood despite their importance for both MgO specifically and for many natural minerals generally. However, the effects of such transformation are different from most ionic crystals investigated by SFM so far, which show uniformly retreating monolayer steps during dissolution (e.g., calcite: Hillner et al. 1992b; Liang et al. 1996). In addition, this phenomenon has broad parallels to the formation of leached or altered layers on silicates (e.g., feldspars: Casey et al. 1989; Chou and Wollast 1985; Hellmann et al. 1990), and thus is a useful starting place for understanding how to deal with altered layer formation in SFM studies, especially as high-temperature SFM becomes available (Higgins et al. 1998).

EXPERIMENTAL METHODS

Periclase has the rock salt structure (space group: $4/m\bar{3}2/m$) with a lattice constant of $a_0 = 0.42$ nm. There-

* Current address: Institut für Mineralogie und Geochemie, Universität zu Köln, Zülpicher Str. 49 b, 50674 Köln, Germany. E-mail: jordan@min.uni-koeln.de

0003–004X/99/0102–0144$05.00

fore, on the (001) surface the height of monolayers is $a_0/2 = 0.21$ nm. MgO exhibits perfect cleavage on (001). Synthetic crystals from Marketech International were used. The experiments were performed using a Nanoscope-IIIa-Multimode-SFM (Digital Instruments). The images were taken with silicon probes (spring constant: 0.02–0.1 N/m) in contact mode. The loading force applied was smaller than ~10 nN. However, for the acquisition of dissolution rate data, the surface was scanned only about 4 times an hour to reduce the risk of surface alteration induced by the scanning tip (which can introduce systematic errors to the calculation of dissolution rates). The in-situ imaging of the surface during dissolution and measurements of the vertical surface position were carried out with a commercially available fluid cell (Digital Instruments). Solutions were fed into the cell gravimetrically (without stopping flow while images were taken); flow rates ranged from 0.3 mL/min to 6 mL/min. Experiments at pH 2 were conducted with a flow rate of at least 2 mL/min because it was impossible to evaluate any dependence of dissolution rate on flow rate at this pH (see below). The solutions were prepared by using ultra-pure deionized water (resistivity: 18 $M\Omega$ cm) and reagent grade HCl. Experiments were conducted at room temperature (23–24 °C).

Cup-shaped sample holders were made from titanium. The inner diameter of the sample holders is 6.4 mm with a depth of 2 mm. The MgO samples were affixed into these sample holders using epoxy (Dexter Corp.). The crystals were cleaved after the epoxy had set for at least 2 h; final dimensions of the crystals were $\sim 2 \times 0.5 \times 5$ mm. In the fluid cell the (001) surface (0.5×5 mm) was facing toward the tip, the long edge parallel to the cantilever. Corrosion or pitting of the sample holder by the solutions could not be detected.

Results

In general, unreacted MgO (001) cleavage faces were microscopically rough and showed two different patterns. In some cases the cleavage face revealed high steps (up to about 25 nm) in a zigzag pattern. The angles occurring in this pattern are 25–35° (Fig. 1a). But most frequently the surface consisted of parallel steps up to about 10 monolayers in height (~2 nm; Fig. 1b). The observed morphology of the periclase cleavage surface is in agreement with observations of Ikemiya et al. (1996), Perrot et al. (1994), and Sangwal et al. (1997).

Even after exposure to air for about 5 min—the time required for mounting the samples into the microscope—a few protrusions on the surface can be discerned (Fig. 1b). The protrusions are frequently located at the steps but can also be found on terraces. The density of the protrusions varies between 10 and 100 μm^{-2}. The height of the protrusions is about 1 nm. Due to possible tip-surface convolution, only an upper limit of about 20 nm can be assigned to the diameter. As soon as deionized water (pH ~ 5.8) is inserted into the fluid cell of the microscope (Fig. 1c), the protrusions tend to grow in size (up to 5 nm in height) and density (10–150 μm^{-2}). Besides a slight roughening of the surface and the growth of the protrusions, the surface is relatively stable in water (Fig. 1d). Even after a period of 60 min, dissolution is not obvious. However, it cannot be ruled out that the protrusions and the surface roughening might ''screen'' a possible slight movement of steps at terraces.

The surface morphology alters immediately and extensively after exchange of the deionized water in the fluid cell for an HCl solution with pH $\leq$ 3. As soon as the pH of the fluid within the cell decreases, dissolution begins by a further roughening of the surface (Fig. 1e). The protrusions formed in water at a higher pH are removed, individual terraces can no longer be observed, and new asperities are formed. The slopes of these asperities are about 25°. The maximum slopes observed are about 35°. The RMS-roughness of the surface is about 2 nm at pH values from 1 to 3. The maximum relief (vertical distance between high point and low point) is 15 nm. At pH 1 this roughness is reached within seconds [note the roughening evident in Fig. 1e during the down-scan; the subsequent up-scan (Fig. 1f) shows the roughening in the upper part of the image compared to Fig. 1e], whereas at pH 3 it takes up to 10 min to reach this roughness (not shown).

A further difference in the properties of the surface caused by the exchange of deionized water in the fluid cell for an HCl solution with pH $\leq$ 3 is that at low pH the surface appears to be much softer than in deionized water. Even a loading force as small as 10 nN, which does not affect the surface morphology of most ionic solids studied by SFM (e.g., on calcite: Park et al. 1996), causes considerable surface damage manifested by deeply carved scan fields after repeatedly scanning the surface. Therefore, besides the change in surface morphology, low pH solutions alter physical properties of the near surface region of periclase and generate a soft surface layer.

Dissolution mainly takes place by a vertical retreat of the surface while keeping its rough morphology without observable retreat at monolayer steps. To quantify this kind of dissolution, the vertical retreat of the surface can be measured by monitoring the voltage of the z-piezo. This method has been used to quantify dissolution rates (e.g., calcite: Hong et al. 1997). We used 15 $\mu m \times 15$ μm scans of the surface and monitored the median height of the scan field (i.e., 50% of the scan field has a higher and 50% a lower vertical position). Figure 2 shows sequences of the vertical retreat of a periclase (001) surface. The error in acquiring vertical retreat data is caused by several factors, including thermal drift, effects of softening and swelling of the epoxy holding the sample, and fluctuations of the flow rate that cause variation in the vertical deflection signal of the cantilever. Instabilities of the piezo and associated electronics can be neglected as an error source. For example, at pH 1 the full 440 V range of the piezo is passed within about 4 h as a result of dissolution. In contrast, the variation of the vertical deflection signal caused by all error sources typically corresponds to an up- and downward movement of the piezo

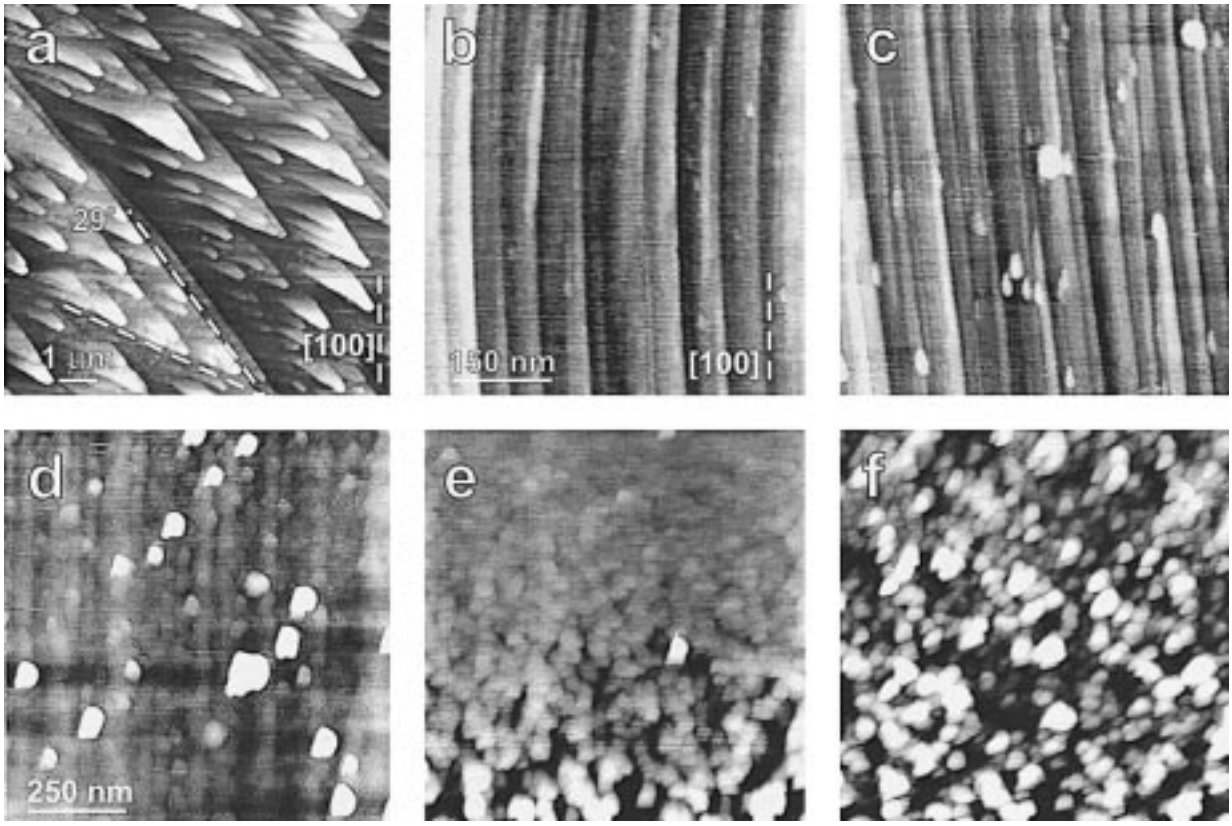

FIGURE 1. (**a**) (001) cleavage face of periclase showing steps arranged in a zigzag pattern (step heights: up to 20 nm; surface was exposed to deionized water for 18 min). (**b**) (001) cleavage face with steps parallel to [100]. The steps consist of 2 to 8 monolayers (the curvature of steps is caused by image drift). On the surface a few protrusions (height = <1 nm) can be discerned (surface was exposed to air for about 30 min). (**c**) After 5 min in deionized water: size and areal density of protrusions grow (same scale as **b**). (**d**–**f**) Same surface area. (**d**) After 61 min in deionized water, the surface has become roughened, steps are poorly resolved, but overall dissolution is not obvious. (**e**) During exchange of deionized water for acidified water (pH 1): In the upper part of the image, the dissolution of the protrusions formed in deionized water and the removal of steps and terraces by surface roughening can be seen. In the lower part of the image surface roughening created a completely different surface morphology (down-scan; image acquisition time = 50 s). (**f**) Immediately successive to **e**: The whole surface is affected by tremendous surface roughening. The slope of the asperities is about 25°; their maximum height is about 15 nm. Due to tip-sample convolution the actual morphology of asperities cannot be resolved (up-scan; image acquisition time = 50 s).

within a range of 30 V (200 nm of topography, see dashed line segments in Fig. 2). In general, the error sources are independent of the pH of the solution applied. Therefore, at low pH the vertical retreat rate is high with respect to the scatter of data (Fig. 2a), whereas at higher pH data scatter becomes more obvious (Fig. 2c).

To monitor scatter of data and possible drift in the vertical direction, the vertical position of the surface can be measured in deionized water (pH ~ 5.8) before and after measuring the vertical retreat rate in the solution of interest. Because dissolution in deionized water is very slow, vertical movement can be attributed to vertical drift and data scatter. However, the vertical retreat rate at pH 3 becomes so slow that even a correction of data by the retreat in deionized water is not helpful—scattering of data around zero screens the actual retreat rate. Therefore, measuring rates by determining the vertical retreat of the surface fails at pH-values higher than 2.

In Table 1 the vertical retreat rates of the periclase (001) surface between pH 1 and 2 are summarized and converted into dissolution rates. Based on the molecular weight (40.3 g/mol) and the specific gravity of periclase (3.6 g/cm^3) a retreat rate of 1 nm/min corresponds to 1.49×10^{-6} mol/m^2·s. However, because of surface area normalization, the roughness of the surface (not considered in these calculations) should lead to slightly lower rates (based on the 25° slope of the surface asperities the actual surface area can be up to 10% larger than the scan area). Also, the measured dissolution rate does not consist exclusively of retreat of a surface with constant roughness, but has a contribution from retreating macro-steps (Figs. 3 and 4). The appearance of steps depends strongly on

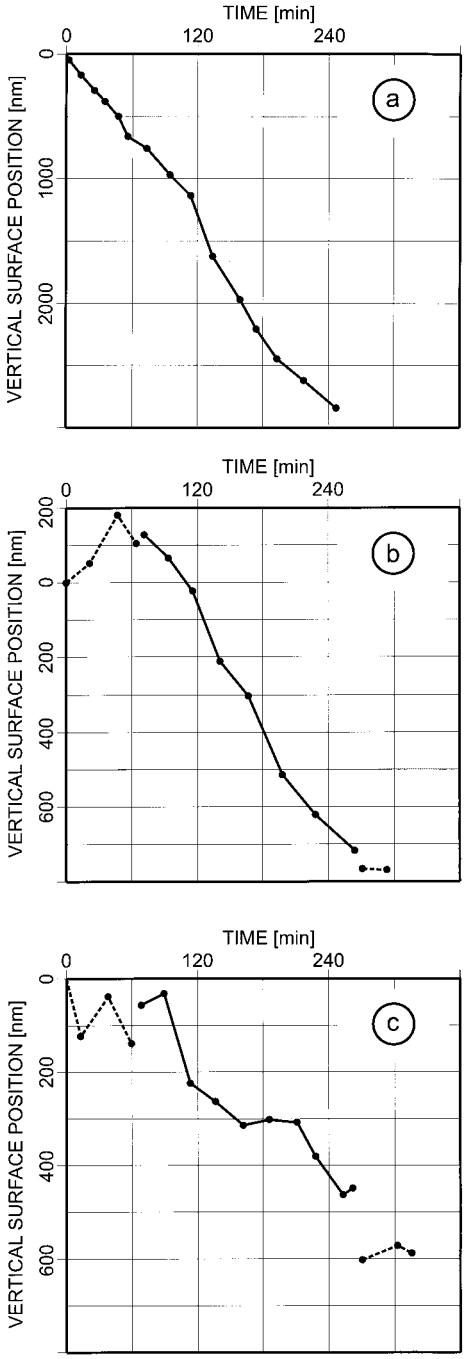

FIGURE 2. Plot of the vertical surface position vs. time. (**a**) pH 1; the data show a fairly constant linear dependence of the surface position on time. The linear regression gives a retreat rate of 12.1 ± 0.3 nm/min. (**b**) pH 1.5 (solid line) and deionized water (dashed line). The linear regression of the advance of the vertical surface position in deionized water at the beginning of the experiment gives 2.2 ± 1.2 nm/min. The retreat rate at pH 1.5 is 4.7 ± 0.2 nm/min. The jumps of the vertical surface position during exchange of the solution are caused by bending of the cantilever induced by the different pH of the solution. (**c**) pH 2 (solid line) and deionized water (dashed line). The regression during the pH 2 stage of experiment gives a retreat rate of 2.0 ± 0.2 nm/min. Regression of the initial stage with deionized water = 1.5 ± 1.5 nm/min.

TABLE 1. Dissolution rates of the periclase (001) surface at pH 1–2

pH	Vertical retreat (nm/min)	Dissolution rate (10^{-6} mol/m^{2}s)	log (rate)
1	11.5 ± 3.9	17.1 ± 5.8	−4.77
1.5	6.1 ± 1.1	9.1 ± 1.6	−5.04
2	3.8 ± 2.5	5.7 ± 3.7	−5.25

Note: The rates were calculated by the vertical retreat of the surface [based on the molecular weight (40.3 g/mol) and the gravity of periclase (3.6 g/cm^3), a retreat rate of 1 nm/min corresponds to 1.49 × 10^{-6} mol/m^2·s].

the pH of the solution. At pH 1 steps with a height up to about 120 nm occur frequently, but at pH 2 only a few small steps are observable. These small steps soon become roughened and eventually unresolvable within the rough surface. Macro-steps generated at pH 1 are not stable at pH 2 and disappear within the rough surface (Figs. 5a–5c).

The macro-steps are usually formed by nucleation of square pits (i.e., macro-steps represent the walls of flat bottomed etch pits). The orientation of the steps is roughly parallel to [110] and equivalent directions, but at the pit edges, steps are frequently rounded. This etch pit shape is in agreement to the results of Sangwal (1980) who reported pits etched at comparable pH-values to be ''<110> pits''. Also, ''two-sided'' pits can be found in which macro-steps occur only along two sides of the pit; the remaining sides of such pits consist of a rough, shallowly inclined surface with no obvious steps (Figs. 5d–5f). Below pH 2, where step edges enable velocity measurements, step retreat shows a clear dependence on pH: at pH 1 the velocity of step retreat is 61 ± 10 nm/min and at pH 1.5 the velocity is 19 ± 15 nm/min. Neither step height nor step spacing (down to about 300 nm) exerted a noticeable influence on step velocities. The large error of these average step velocities is mainly caused by lateral drift: in general, sequences provided neither reference points (such as particles on the surface) nor complete pits to correct the influence of drift for a sufficient period of time. Furthermore, it cannot be ruled out that different amounts of unknown impurities in different experiments (e.g., Derksen et al. 1994) caused an additional variation in step velocities. However, measurements of the velocity while changing the flow rate of solution through the fluid cell can be used as a sensitive indication of a possible dependence of the dissolution rate on the flow rate. In the range of flow rates used (0.3–6 mL/min), no such dependence was detected. Due to the lack of steps at pH 2, this method is limited to the experiments conducted at lower pH-values. To avoid flow-rate dependent dissolution rates at pH 2, experiments were conducted with a flow rate of at least 2 mL/min. Judging by the dissolution rate at pH 1 and the dimensions of the samples, the release of dissolved material into the fluid cell is about 5 × 10^{-10} mol/s. Without flow through the cell this release rate would cause a MgO concentration of ~ 10^{-5} *M* in one second. Applying a flow rate of 2

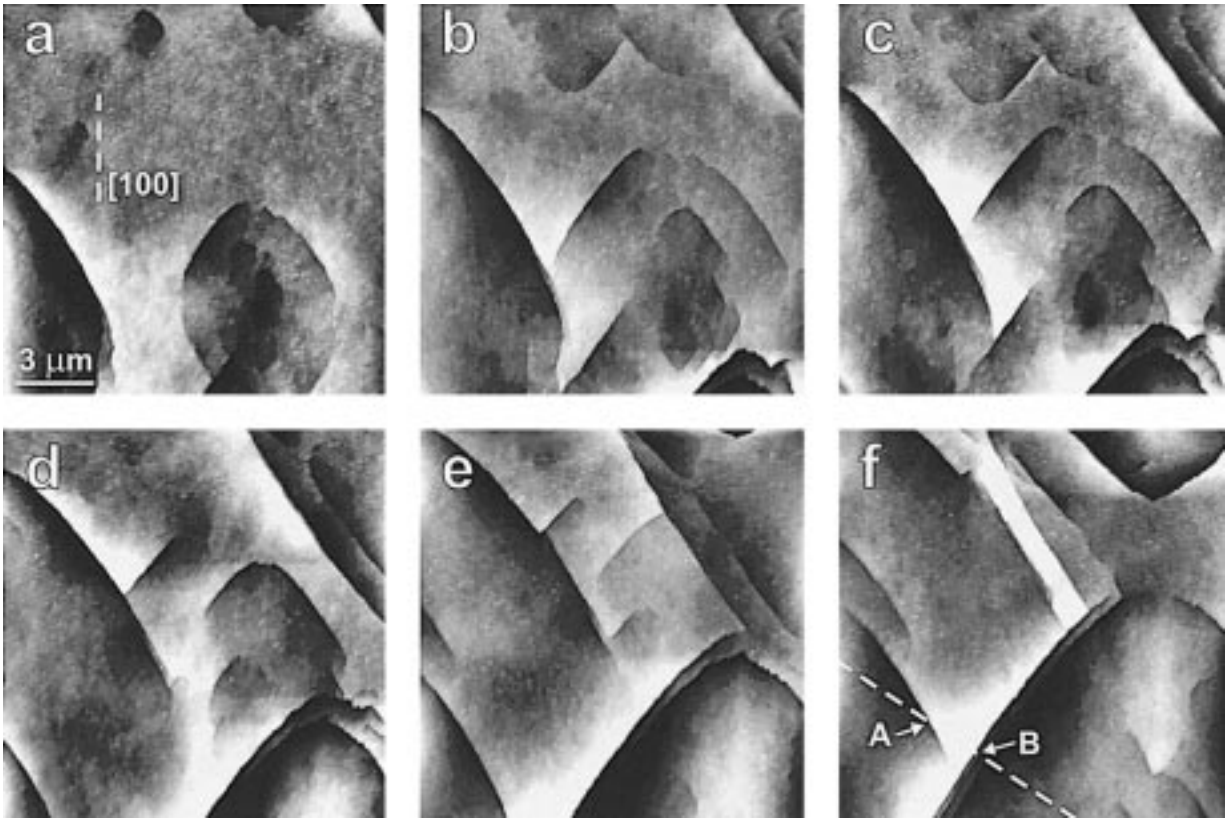

FIGURE 3. Sequence of the periclase (001) surface during dissolution at pH 1. Large steps (i.e., pit walls—in this sequence up to 80 nm in height) are formed by pits on the surface. The step edges are aligned parallel to [110] and equivalent directions. The slope of step edges reaches angles (here) up to 40°. (**a**) 0 min; (**b**) 31 min; (**c**) 39 min; (**d**) 57 min; (**e**) 76 min; (**f**) 99 min (the line indicates the position of the section in Fig. 4; A and B mark the steps in the section; note that B refers to 3 close steps).

mL/min, the volume of new solution which is fed into the fluid cell equals the volume of the fluid cell in 2 s. Therefore, saturation effects on dissolution rate are highly unlikely as supported by the independence of step velocities with flow rate at pH < 2.

The slope of the data in the log (rate) vs. pH diagram (Fig. 6) has been used as an indication of the rate-determining step of dissolution (e.g., Vermilyea 1966, 1969). However, due to the large errors in the rates, the slope must be regarded as an estimation; an unweighted linear regression of the data yields -0.48 ± 0.04, but the data are permissive of slopes between -0.1 and -1.1.

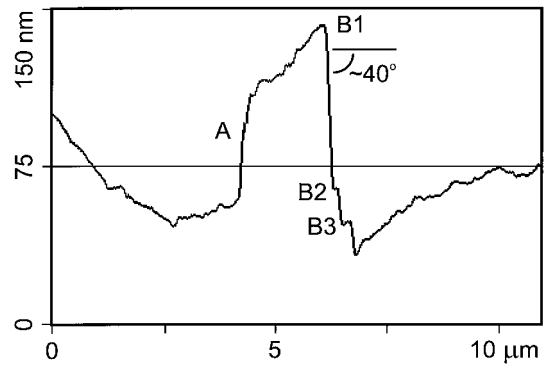

FIGURE 4. Section of Figure 3f. The entire height of the 3 steps marked B1 to B3 is ~110 nm, the slope between B1 and B2 is about 40°.

DISCUSSION

The observed initial roughening of the periclase (001) surface in air and water was previously reported. Holt et al. (1997) presented various surface features generated by different humidity and temperature conditions, and protrusions similar to those in our study can be found in their images. Jones et al. (1981, 1984) observed a roughened surface by electron microscopy both at water vapor pressures of $<10^{-5}$ Pa and in water before any significant dissolution took place, and referred to this surface morphology as ''castellated''. Furthermore, they showed by infrared spectroscopic studies that there is a clear correlation among the surface roughening, surface defects (i.e., low-coordination surface sites—terrace vacancies, steps, and kinks), and an increase in ν(OH) absorption. Further support for the correlation of surface defect sites with surface hydroxyl groups comes from theoretical calculations by Scamehorn et al. (1993, 1994), Langel and Par-

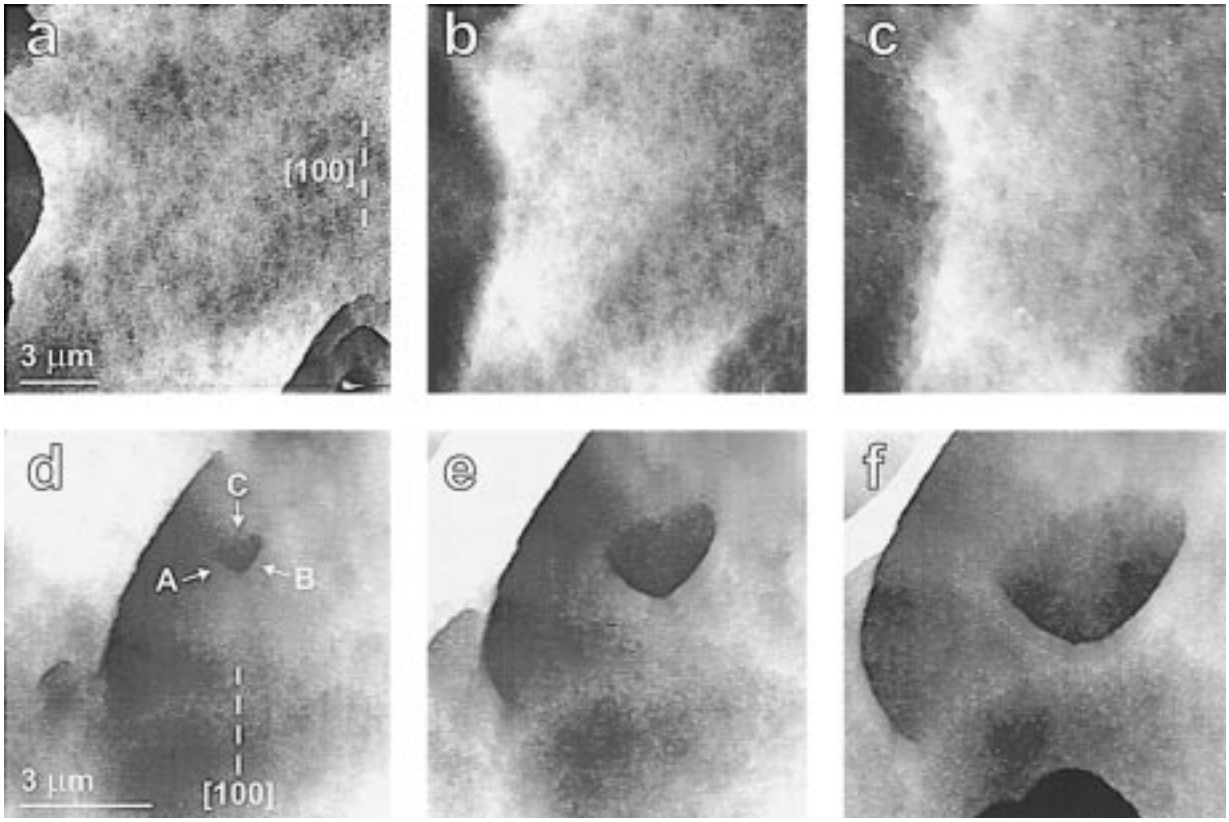

FIGURE 5. (**a**–**c**) Macro-steps at pH 1 and 2. (**a**) At pH 1 macro-steps show sharp edges. The step heights in the image are up to 70 nm. (**b**) 104 min at pH 2: the edges of macro-steps are rounded. (**c**) 209 min at pH 2: instead of macro-steps only transition zones between the former terraces can be observed. The transition zones have a width of about 2 μm. (**d**–**e**) Growing asymmetric (''two-sided'') pit at pH 1 (labeled A–C). The lower two sides of the pit (A and B) formed macro-steps, but the upper side of the pit (C) is shallowly inclined and rough. Even within this shallow slope no steps can be observed. (**d**) 0 min; (**e**) 14 min; (**f**) 30 min.

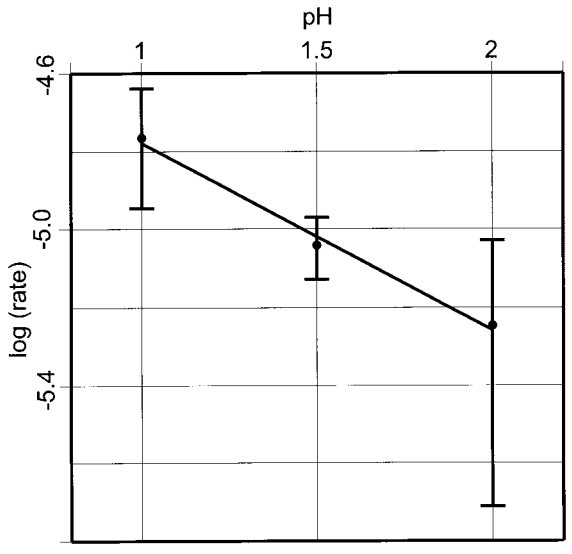

FIGURE 6. Plot of the logarithm of dissolution rates (mol/m^2·s) (as measured by rate of vertical retreat of the surface) vs. the pH of solution. The slope of the linear regression of the data points is -0.48 ± 0.04.

inello (1994), and Refson et al. (1995). They showed that on the perfect MgO (001) surface H_2O physisorbs readily, while dissociative chemisorption of H_2O is energetically favored at low-coordinated surface defect sites only. Therefore (despite the possibility that the protrusions consist of Mg-carbonates generated by ambient CO_2), it seems likely that surface hydroxyl groups give rise to protrusions consisting of poorly ordered hydroxide (perhaps a brucite precursor).

As soon as acidified water enters the fluid cell, the situation changes completely. At low pH, Wogelius et al. (1995) found protonation of periclase not only on the surface but also in the near-surface region. This protonated near surface region is likely reflected by the soft surface layer detectable by contact mode SFM. Considering the mechanism, Wogelius et al. (1995) suggested that a replacement of Mg^{2+} by H^+ along the (111) planes of periclase creates penetrative brucite (001)-like layers. Periclase and brucite have close structural similarities, and a well-known epitaxial relationship between the periclase (111) surface and the brucite (001) surface exists (Giovanoli et al. 1968; Goodman 1958). Replacing every Mg atom in a periclase (111) plane with two protons gives a

d spacing within 2% of the brucite (001) *d* spacing (Wogelius et al. 1995). However, to obtain a perfect brucite lattice, only every second Mg-layer has to be replaced. Because protonation probably does not occur in such an ordered fashion, the surface structure is likely to be ordered poorly (despite H/Mg ratios even up to the ratio of brucite could be detected in the near surface region by Wogelius et al. 1995). Furthermore, perfect ordered brucite layers on periclase would demand a surface hardness comparable to the brucite (001) surface. The surface of periclase (001) at low pH, however, is much softer than the brucite (001) surface (on brucite loading forces $\leq$10 nN did not cause observable surface damage; Jordan and Rammensee 1996).

Hydroxylation of periclase stabilizes the (111) surface. Refson et al. (1995) have shown that a hydroxylated periclase (001) surface (e.g., by protonation of surface oxygen) is energetically unfavorable and thus less stable than the hydroxylated (111) surface. Therefore, we suggest that due to the protonation of the near-surface region, the (001) surface is probably quickly restructured into a poorly ordered, facetted (111) surface [even in the shallow inclined parts of newly formed, asymmetric pits, smooth terraces parallel to (001) cannot be observed; Figs. 5d–5f]. Due to tip-surface convolution the presumed (111) nano-facets cannot be imaged by SFM. Instead of facets, images show round asperities with reduced slope. The rounded pattern in Figure 1f is typical for scanning a surface with a dull, rounded tip. Tip-surface convolution is a general problem encountered while scanning the altered periclase surface due to the soft surface (which may cause adhesion of material from the surface to the tip). However, using SEM, Wogelius et al. (1995) detected a ''mottled'' surface after etching periclase in pH 2 and 4. The macro-steps generated by pits (i.e., the walls of flat bottomed etch pits) represent larger (111) facets (Fig. 3). The slope of these steps (up to 50° with respect to (001) can be found) is lower than the theoretical slope (55°) of a (111) facet. The likely reason for this difference is that within these facets microtopography can be formed, which causes a reduced slope. The microtopography can be caused by preferential dissolution at the upper edge of the pit walls and by the lack of structural order achieved while protonation takes place down into the near-surface region. A less ordered structure should not be able to form perfect (111) terraces during dissolution. Finally, tip-surface convolution may also contribute to lower slopes.

The existence of a brucite-like surface layer on periclase during dissolution at low pH was suggested by Vermilyea (1969), who found similar dissolution rates for MgO and $Mg(OH)_2$ at pH $<$ 5. Using periclase powder, he determined the dissolution rate to be $\sim 2 \times 10^{-4}$ mol/m^2·s at pH 2 (+0.1 *M* KCl). This result is considerably faster than the results of Segall et al. (1978), 9.5×10^{-6} mol/m^2·s (MgO smoke cubes, HNO_3), Wogelius et al. (1995), 7.2×10^{-6} mol/m^2·s (single crystal, HNO_3), and our data of the (001) surface, 5.7×10^{-6} mol/m^2·s. The difference of the rate reported by Vermilyea (1969) to the other rates is most likely due to the usual problems of surface area normalization (Vermilyea calculated the surface area from the particle size) and the contributions of surfaces other than (001) in powder experiments. At pH 1 (single crystal, HCl), Sangwal and Arora (1978) found a rate of $\sim 2 \times 10^{-5}$ mol/m^2·s (assuming the data point in the their diagram to be at $\sim 2.8 \times 10^{-4}$ g/cm^2·h). Although this rate is in excellent agreement with our rate (1.71×10^{-5} mol/m^2·s), their ''lateral etch rate'' measured at etch pits ($\sim$150 nm/min) is about 2.5 times larger than the retreat of pit walls (i.e., velocity of macro-steps) in our experiments. Using SFM on brucite (001), Jordan and Rammensee (1996) found a rate of $\sim 1 \times 10^{-6}$ mol/m^2·s at pH 2.7 (23–24 °C). Extrapolating our periclase (001) data to the pH-value of 2.7 by applying the slope -0.48 of the regression in the log (rate) vs. pH diagram (Fig. 6) gives a dissolution rate of 2.5×10^{-6} mol/m^2·s, which is similar to that of Jordan and Rammensee (1996) and, therefore, gives further support to the idea that the periclase (001) surface consists of brucite-like protonation products. The high activation energy for dissolution of brucite and the fact that well-ordered brucite (001) layers show evidence for interstep-interaction makes it likely that surface diffusion contributes to the rate-determining step of dissolution of the brucite (001) surface (Jordan and Rammensee 1996). We speculate that the high defect density of the presumably poorly ordered hydroxide layers on periclase leads to accelerated dissolution rates that overcome any limitation imposed by surface diffusion.

The slope of log (rate) vs. pH should give information about the rate-determining step of dissolution. Despite similar results to ours in the literature, this situation also remains ambiguous. Vermilyea (1969) found a slope of -0.47 and claimed that this is consistent with the protonation of surface hydroxyl groups as rate determining step. Segall et al. (1978) reported the slope to be -0.49 and argued that due to the modification of the surface potential barrier by protons, cation removal is the most likely rate-determining step. Jones et al. (1981) suggested the reaction $O^{2-} + H^+ \rightarrow OH^-$ (causing a slope of -0.5) as rate-determining after an initial stage of dissolution. However, in the light of the fast protonation not only of the surface but also of the near-surface region at pH 2, this reaction is unlikely to be the rate-determining step.

The results of this study have implications for other solids, such as feldspars, that may undergo surface alteration during dissolution. The kinematic constraints imposed by a well-ordered surface structure (e.g., with well-defined steps and monolayer step retreat) largely break down upon alteration and roughening. Retreat of altered, roughened surfaces may be more common during the dissolution of many naturally occurring minerals than previously suspected.

Acknowledgments

We are grateful to the NSF (EAR-9634143) for support of the SFM purchase. We also thank the office of Basic Energy Science (DOE) for

partial support of this research (no. DE-FG03-965F/4623/A000). G.J. is grateful to the DAAD (German Academic Exchange Service, Hochschulsonderprogramm III von Bund und Ländern) for financial support. The thorough reviews by Kathryn Nagy, Richard Reeder, and Roy Wogelius are highly appreciated.

References cited

Berner, R.A. (1995) Chemical weathering and its effect on atmospheric CO_2 and climate. In Mineralogical Society of America Reviews in Mineralogy, 31, 565–583.

Bosbach, D. and Rammensee, W. (1994) In situ investigation of growth and dissolution on the (010) surface of gypsum by Scanning Force Microscopy. Geochimica et Cosmochimica Acta, 58, 843–849.

Casey, W.H., Westrich, H.R., Arnold, G.W., and Banfield, J.F. (1989) The surface chemistry of dissolving labradorite feldspar. Geochimica et Cosmochimica Acta, 53, 821–832.

Chou, L. and Wollast, R. (1985) Steady-state kinetics and dissolution mechanisms of albite. American Journal of Science, 285, 963–993.

Derksen, A.J., van Enckevort, W.J.P., and Couto, M.S. (1994) Behaviour of steps on the (001) face of $K_2Cr_2O_7$ crystals. Journal of Physics D: Applied Physics, 27, 2580–2591.

Giovanoli, R., Feitknecht, W., and Fahrer, W. (1968) Über das epitaktische Aufwachsen von Magnesiumhydroxid auf Magnesiumoxid. Journal de Microscopie, 7, 177–194.

Goodman, J.F. (1958) The decomposition of magnesium hydroxide in an electron microscope. Proceedings of the Royal Society of London, A247, 346–352.

Gratz, A.J., Manne, S., and Hansma, P. (1990) Atomic force microscopy of atomic-scale ledges and etch pits formed during dissolution of quartz. Science, 251, 1343–1346.

Hellmann, R., Eggleston, C.M., Hochella, M.F. Jr., and Crerar, D.A. (1990) The formation of leached layers on albite surfaces during dissolution under hydrothermal conditions. Geochimica et Cosmochimica Acta, 54, 1267–1281.

Higgins, S.R., Eggleston, C.M., Knauss, K.G., and Boro, C.O. (1998) A hydrothermal atomic force microscope for imaging in aqueous solution up to 150°C. Review of Scientific Instruments, 69, 2994–2998.

Hillner, P.E., Gratz, A.J., Manne, S., and Hansma, P.K. (1992a) Atomic scale imaging of calcite growth and dissolution in real time. Geology, 20, 359–362.

Hillner, P.E., Manne, S., Gratz, A.J., and Hansma, P.K. (1992b) AFM images of dissolution and growth on a calcite crystal. Ultramicroscopy, 42–44, 1387–1393.

Holt, S.A., Jones, C.F., Watson, G.S., Crossley, A., Johnston, C., Sofield, C.J., and Myhra, S. (1997) Surface modification of MgO substrates from aqueous exposure: an atomic force microscopy study. Thin Solid Films, 292, 96–102.

Hong, Q., Suarez, M.F., Coles, B.A., and Compton, R.G. (1997) Mechanism of solid/liquid interfacial reactions. The maleic acid driven dissolution of calcite: An atomic force microscopy study under defined hydrodynamic conditions. Journal of Physical Chemistry, B 101, 5557–5564.

Ikemiya, N., Kitamura, A., and Hara, S. (1996) Surface structures of MgO(100) and $SrTiO_3$(100) as revealed by atomic force microscopy. Journal of Crystal Growth, 160, 104–110.

Jones, C.F., Segall, R.L., Smart, R.S.C., and Turner, P.S. (1981) Initial dissolution kinetics of ionic oxides. Proceedings of the Royal Society of London, A374, 141–153.

Jones, C.F., Reeve, R.A., Rigg, R., Segall, R.L., Smart, R.S.C., and Turner, P.S. (1984) Surface area and the mechanism of hydroxylation of ionic oxide surfaces. Journal of the Chemical Society, Faraday Transactions I, 80, 2609–2617.

Jordan, G. and Rammensee, W. (1996) Dissolution rates and activation energy for dissolution of brucite (001): A new method based on the microtopography of crystal surfaces. Geochimica et Cosmochimica Acta, 60, 5055–5062.

———(1998) Dissolution rates of calcite ($10\bar{1}4$) obtained by scanning force microscopy: microtopography based dissolution kinetics on surfaces with anisotropic step velocities. Geochimica et Cosmochimica Acta, 62, 941–947.

Langel, W. and Parrinello, M. (1994) Hydrolysis at stepped MgO surfaces. Physical Review Letters, 73, 504–507.

Liang, Y., Baer, D.R., McCoy, J.M., Amonette, J.E., and LaFemina, J.P. (1996) Dissolution kinetics at the calcite-water interface. Geochimica et Cosmochimica Acta, 60, 4883–4887.

Park, N.S., Kim, M.W., Langford, S.C., and Dickinson, J.T. (1996) Tribological enhancement of $CaCO_3$ dissolution during scanning force microscopy. Langmuir, 12, 4599–4604.

Perrot, E., Dayez, M., Humbert, A., Marti, O., Chapon, C., and Henry, C.R. (1994) Atomic-scale resolution on the MgO (100) surface by scanning force and friction microscopy. Europhysics Letters, 26, 659–663.

Refson, K., Wogelius, R.A., Fraser, D.G., Payne, M.C., Lee, M.H., and Milman, V. (1995) Water chemisorption and reconstruction of the MgO surface. Physical Review B, 52, 10823–10826.

Roy, D.M., Roy, R., and Osborn, E.F. (1953) The system MgO-Al_2O_3-H_2O and the influence of carbonate and nitrate ions on the phase equilibria. American Journal of Science, 251, 337–361.

Sangwal, K. (1980) On the adsorption processes in the selective etching of MgO and CaF_2 crystals. Journal of Materials Science Letters, 15, 522–525.

Sangwal, K. and Arora, S.K. (1978) Etching of MgO crystals in acids: kinetics and mechanism of dissolution. Journal of Materials Science, 13, 1977–1985.

Sangwal, K., Sanz, F., Sevat, J., and Gorostiza, P. (1997) Nature of multilayer steps on the {100} cleavage planes of MgO single crystals. Surface Science, 383, 78–87.

Scamehorn, C.A., Hess, A.C., and McCarthy, M.I. (1993) Correlation corrected periodic Hartree-Fock study of the interactions between water and the (001) magnesium oxide surface. Journal of Chemical Physics, 99, 2786–2795.

Scamehorn, C.A., Harrison, N.M., and McCarthy, M.I. (1994) Water chemistry on surface defect sites: Chemidissociation versus physisorption on MgO (001). Journal of Chemical Physics, 101, 1547–1553.

Segall, R.L., Smart, R.S.C., and Turner, P.S. (1978) Ionic oxides: Distinction between mechanisms and surface roughening effects in the dissolution of magnesium oxide. Journal of the Chemical Society, Faraday Transactions I, 74, 2907–2912.

Stumm, W., Ed. (1985) Chemical Processes in Lakes, 435 p. Wiley-Interscience, New York.

———(1987) Aquatic Surface Chemistry, 520 p. Wiley-Interscience, New York.

Sverdrup, H.U. (1990) The kinetics of the base cation release due to chemical weathering, 246 p. Lund University Press, Lund, Sweden.

Vermilyea, D.A. (1966) The dissolution of ionic compounds in aqueous media. Journal of the Electrochemical Society, 113, 1067–1070.

———(1969) The dissolution of MgO and $Mg(OH)_2$ in aqueous solution. Journal of the Electrochemical Society, 116, 1179–1183.

Watson, G., Holt, S.A., Zhoa, R.-P., Katsaros, A., Savvides, N., and Myhra, S. (1995) Environmental degradation of $YBa_2Cu_3O_{7-x}$ thin films. Analysis by atomic force microscopy. Physica C, 243, 123–133.

White, A.F. and Brantley, S.L., Eds. (1995) Chemical Weathering Rates of Silicate Minerals. In Mineralogical Society of America Reviews in Mineralogy, 31.

Wogelius, R.A., Refson, K., Fraser, D.G., Grime, G.W., and Goff, J.P. (1995) Periclase surface hydroxylation during dissolution. Geochimica et Cosmochimica Acta, 59, 1875–1881.

Manuscript received April 8, 1998
Manuscript accepted August 28, 1998
Paper handled by Kathryn L. Nagy